Journal of Molecular Structure 1105 (2016) 403–414

Contents lists available at ScienceDirect

Journal of Molecular Structure

journal homepage: http://www.elsevier.com/locate/molstruc

Structural, electronic, topological and vibrational properties of a series of N-benzylamides derived from Maca (*Lepidium meyenii*) combining spectroscopic studies with ONION calculations

Fernando E. Chain [a], María Florencia Ladetto [b], Alfredo Grau [c], César A.N. Catalán [a], Silvia Antonia Brandán [b, *]

[a] INQUINOA-CONICET, Instituto de Química Orgánica, Facultad de Bioquímica Química y Farmacia, Universidad Nacional de Tucumán, Ayacucho 471, 4000. S. M. de Tucumán, Tucumán, Argentina
[b] Cátedra de Química General, Instituto de Química Inorgánica, Facultad de Bioquímica, Química y Farmacia, Universidad Nacional de Tucumán, Ayacucho 471, 4000. San Miguel de Tucumán, Tucumán, Argentina
[c] Instituto de Ecología Regional (IER), Facultad de Ciencias Naturales, Universidad Nacional de Tucumán, C.C. 34, 4107 Yerba Buena, Tucumán, Argentina

ARTICLE INFO

Article history:
Received 27 July 2015
Received in revised form
22 October 2015
Accepted 26 October 2015
Available online 30 October 2015

Keywords:
N-benzylamides
Vibrational spectra
Molecular structure
Force field
DFT calculations

ABSTRACT

In the present work, the structural, topological and vibrational properties of four members of the N-benzylamides series derived from Maca (*Lepidium meyenii*) whose names are, N-benzylpentadecanamide, N-benzylhexadecanamide, N-benzylheptadecanamide and N-benzyloctadecanamide, were studied combining the FTIR, FT-Raman and ^{1}H and ^{13}C-NMR spectroscopies with density functional theory (DFT) and ONION calculations. Furthermore, the N-benzylacetamide, N-benzylpropilamide and N-benzyl hexanamide derivatives were also studied in order to compare their properties with those computed for the four macamides. These seven *N*-benzylamides series have a common structure, C_8H_8NO-R, being R the side chain [$-(CH_2)_n-CH_3$] with a variable n number of CH_2 groups. Here, the atomic charges, molecular electrostatic potentials, stabilization energies, topological properties of those macamides were analyzed as a function of the number of C atoms of the side chain while the frontier orbitals were used to compute the gap energies and some descriptors in order to predict their reactivities and behaviors in function of the longitude of the side chain. Here, the force fields, the complete vibrational assignments and the corresponding force constants were only reported for *N*-benzylacetamide, *N*-benzyl hexanamide and N-benzylpentadecanamide due to the high number of vibration normal modes that present the remains macamides.

1. Introduction

As part of our investigations on compounds with pharmacological and medicinal interest [1–4], in this work, we report the study of a series of four N-benzylamides derived from Maca (*Lepidium meyenii*) that have a common structure: C_8H_8NO-(Ph–CH_2–NH–CO–) attached to an alkyl group R=–$(CH_2)_n$–CH_3 of variable length where the n number of CH_2 groups in the side chain goes from 13 to 16 or from 14 to 17C atoms, whose names are, N-benzylpentadecanamide (IV), N-benzylhexadecanamide (V), N-benzylheptadecanamide (VI) and N-benzyloctadecanamide (VII) (Fig. 1). The structural and vibrational properties of these compounds could be interesting taking into account that many works on the powerful antioxidant activity of the products isolated from Maca [5–8] were published and, also because these products are used to improve the fertility in humans and animals [9–12]. Additionally, some derivatives such as, α-substituted acetamido-*N*-benzylacetamide derivatives can act as anticonvulsant drug class, as reported by Jin et al. [13] and Prichard [14]. In this sense, it is interesting to know the modifications of those properties when changing the quantity of C atoms in the side chain including the vibrational and NMR spectra that are normally employed to their identifications. Numerous products can be extracted from Maca, as reported in the literature [15–20]. Recently, the isolation of some benzylated alkamides, named macamides were reported by Zao et al. [20] and Chain et al. [21] however, in these studies the

* Corresponding author.
E-mail address: sbrandan@fbqf.unt.edu.ar (S.A. Brandán).

http://dx.doi.org/10.1016/j.molstruc.2015.10.082
0022-2860/

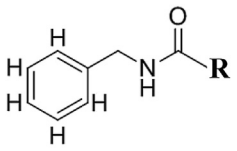

C_8H_8NO-R

R=CH_3 (I) N-benzylacetamide

R= CH_2-CH_3 (II) N-benzylpropanamide

R= $(CH_2)_4$-CH_3 (III) N-benzylhexanamide

R= $(CH_2)_{13}$-CH_3 (IV) N-benzylpentadecanamide

R= $(CH_2)_{14}$-CH_3 (V) N-benzylhexadecanamide

R= $(CH_2)_{15}$-CH_3 (VI) N-benzylheptadecanamide

R= $(CH_2)_{16}$-CH_3 (VII) N-benzyloctadecanamide

Fig. 1. Molecular Formula and names of the series of seven *N*-Benzylamides studied.

different compounds isolated only were characterized by infrared, NMR and UV spectroscopies but their corresponding IR spectra were not presented neither assigned. Hence, in this work, we present a theoretical structural and experimental vibrational study on a series of four macamides, N-benzylpentadecanamide (IV), N-benzylhexadecanamide (V), N-benzylheptadecanamide (VI) and N-benzyloctadecanamide (VII) combining the theoretical DFT/ONION calculations in gas phase with the infrared and Raman spectra in order to calculate the more stable structures of each species and to perform the complete assignments of the bands observed to the normal vibration modes. For these purposes, the different structures were optimized by using ONION/B3LYP/6-31G* calculations [22–24] in gas phase and then, the structural properties such as, atomic charges, molecular electrostatic potentials, stabilization energies, topological properties of those macamides were calculated by using the NBO [25,26] and AIM [27,28] methodologies. Here, the more simple counterparts N-benzylacetamide (I), N-benzylpropanamide (II) and N-benzyl hexanamide (III) were also optimized in order to compare their properties with those corresponding to the four macamides because in their structures there are side chains with one, two and five C atoms respectively. Later, all the properties were analyzed in function of the number of C atoms of the side chain. In addition, the frontier orbitals [29] were used to compute the gap energies together with some interesting descriptors [2,3] in order to predict the reactivities and behaviors of those macamides as a function of the longitude of the side chain. Hence, the modifications in the properties were graphically presented as a function of the lengthening of the side chain because this way, it is possible to observe clearly the changes performed. On the other hand, the internal normal coordinates for N-benzylacetamide, N-benzylpropanamide and N-benzyl hexanamide, the SQM methodology [30], and the Molvib program [31] were employed to perform the assignments of the vibration normal modes of the four N-benzylamides taking as base the assignments of those three basic molecules. Here, we have presented for the first time a new methodology to perform the assignment of molecules containing a long side chain by comparison with similar molecules containing a shorter one.

2. Experimental section

The four macamides N-benzylpentadecanamide (IV), N-benzylhexadecanamide (V), N-benzylheptadecanamide (VI) and N-benzyloctadecanamide (VII) were extracted and isolated from *Lepidium meyenii* Walpers (Brassicaceae) according to the procedure described in Ref. [21]. The characterizations were previously carried out by the ^{1}H NMR and ^{13}C NMR spectra recorded in $CDCl_3$, the FTIR spectra of the samples in KBr pellets and the UV spectra of the compounds in hexane solutions. The FT-Raman spectrum of the samples in solid phases were recorded in the range 4000–50 cm^{-1} using a Bruker RFS 100/s FT-Raman spectrophotometer with a 1064 nm Nd:Yag laser source of 150 mW power. Spectra were recorded with a resolution of 1 cm^{-1} and 200 scans.

3. Computational details

The initial structures of those four macamides, N-benzylpentadecanamide (IV), N-benzylhexadecanamide (V), N-benzylheptadecanamide (VI) and N-benzyloctadecanamide (VII) were modeled with the *GaussView* program [32] and then, their corresponding optimizations were performed by the hybrid B3LYP/6-31G* method and ONION calculations with the Gaussian 09 program [33]. It is necessary to clarify that the computational cost for all the four macamides was notably reduced by using the ONION calculations [22]. The other three, i. e., N-benzylacetamide (I), *N*-benzylpropanamide (II) and N-benzyl hexanamide (III) structures were also optimized at the same level of theory. Thus, Fig. 2 shows only the optimized (II) and (III) structures together with the labeling of the atoms while the common skeleton for all the series of seven N-benzylamides studied is presented in Fig. 1 together with the corresponding names and Molecular Formulas. The numeration of all the atoms remains constant from the first structure and it increases according to the number of C atoms in the side chain up to the N-

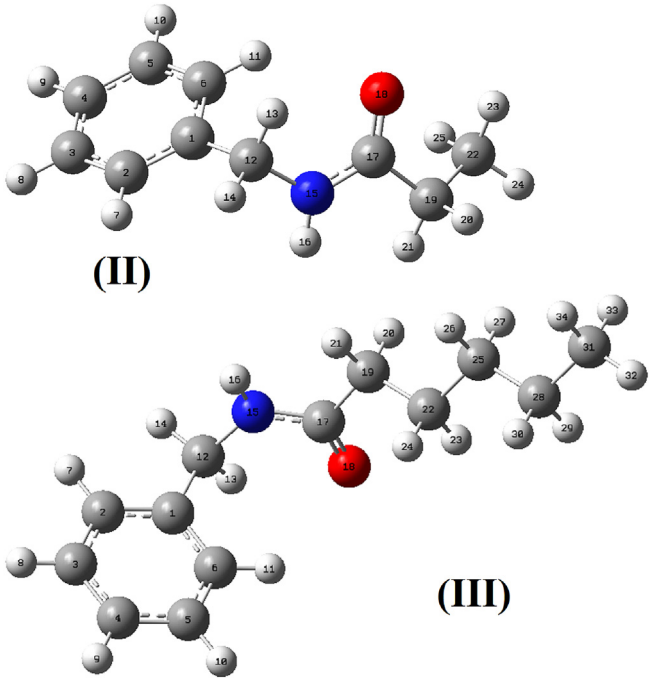

Fig. 2. Comparison between the theoretical molecular structures of N-benzylpropilamide (II) and N-benzyl hexanamide (III) and the atoms numbering.

benzyloctadecanamide (VII). The NBO [25,26] and AIM [27,28] methodologies were used to compute the atomic charges, molecular electrostatic potentials, stabilization energies and topological properties of those amides and macamides by using the same level of theory. The chemical shifts of the ^{1}H NMR and ^{13}C NMR spectra were calculated by using the GIAO method [34] and TMS as reference at B3LYP/6-31G* level of theory. The ultraviolet–visible spectrum was predicted using TD-DFT calculations at the B3LYP/6-31G* theory level with the Gaussian 09 program [33]. Additionally, the internal normal coordinates for *N*-benzylacetamide, *N*-benzylpropilamide and *N*-benzylhexanamide, were used together with the SQM methodology [30] and the Molvib program [31] to perform the assignments of the vibration normal modes of all the *N*-benzylamides series. The internal coordinates only for the compound (III) are presented in Table S1 because the differences with the other compounds are in the coordinates corresponding to the CH_2 groups. The gap energy values of all the species together with some important descriptors were calculated from the corresponding frontier orbitals. Here, the properties were graphically presented in function of the number of C atoms of the side chain in order to analyze their behaviors when increasing the quantity of CH_2 groups in the skeleton.

4. Results and discussion

4.1. Geometry optimization

The calculated geometrical parameters for all the series of N-benzylamides studied using the B3LYP/6-31G* method were compared in Table 1 with those experimental determined recently by Wang et al. [35] by means of X-ray diffraction for bis[N-benzyl-2-(quinolin-8-yloxy)- acetamide] monohydrate and, with the experimental N-benzylacetamide structure reported by Smiszek-Lindert and Kusz [36]. Hence, experimentally, the molecules of N-benzylacetamide are inter-connected by a framework of weak inter-molecular N–H···O hydrogen bonds [36]. Here, the comparisons, expressed in terms of root-mean-square deviation (RMSD) values, show that the bond lengths have a better correlation (0.025–0.022 Å) than the bond angles (1.9–1.7°) using the B3LYP/6-31G* calculation level. Besides, for the amide (I) the values show an enhanced correlation in the bond lengths and angles than the other ones, as expected because the compound compared is an N-benzylacetamide as the compound (I). Note that the higher RMSD differences are observed in the dihedral angles because the C2–C1–C12–N15 and C6–C1–C12–N15 angles for all the amide series are predicted by the calculations different from the experimental ones, with RMSD values between 47.6 and 46.1°. Thus, the amide (I) shows the better approximation for the same reason above explained. The calculated total energy, dipolar moment and volume values for the N-benzylamides series studied can be seen in Table S2. The graphic of the three properties against to the number of C atoms in the side chain is shown in Fig. S1. The behaviors of the energy and volume values of all the amides series with the increase of C atoms in the side chain are completely lineal in both cases, with a correlation coefficient of 1 for E and of 0.9973 for V, as observed in Fig. S1. Note that the E values decrease whiles the V values increase, as expected due to the increasing of CH_2 groups in the side chain. On the other hand, the dipole moment decreases significantly as the length of the side chain increases. In particular, for a side chains of 15C atoms the value is lower than a side chain of 16C atoms. Here, the low density value in the bond critical point (BCP) of N-benzylheptadecanamide explains its low dipole moment value, as will see later in the Aim study.

4.2. Electrostatic potential, charges, and bond orders

There are many references on the antioxidant activity of the macamides to improve energy and modulate the response against oxidative stress [5–7] but, so far, these properties were not theoretically justified. Probably, the structural requirement for the

Table 1
Calculated geometrical parameters for the series of seven N-benzylamides studied.

B3LYP/6-31G*[a]								Exp.[b]
Parameters	I	II	III	IV	V	VI	VII	
Bond lengths (Å)								
C1–C12	1.517	1.517	1.517	1.517	1.517	1.517	1.517	1.508
C12–N15	1.461	1.461	1.461	1.461	1.461	1.461	1.461	1.454
N15–C17	1.368	1.368	1.368	1.368	1.368	1.368	1.368	1.327
C17–O18	1.226	1.227	1.227	1.227	1.227	1.227	1.227	1.226
C17–C19	1.521	1.528	1.527	1.527	1.527	1.527	1.527	1.501
C19–C22	1.094[c]	1.530	1.534	1.534	1.534	1.534	1.534	
C1–C2	1.398	1.398	1.398	1.398	1.398	1.398	1.398	1.367
C1–C6	1.403	1.403	1.403	1.403	1.403	1.403	1.403	1.375
RMSD	0.022	0.025	0.025	0.025	0.025	0.025	0.025	
Bond angles (°)								
C6–C1–C2	118.9	118.9	118.9	118.9	118.9	118.9	118.9	118.1
C1–C12–N15	113.7	113.6	113.6	113.5	113.5	113.6	113.6	113.7
C12–N15–C17	122.1	122.4	122.3	122.4	122.4	122.4	122.4	121.6
N15–C17–O18	122.8	122.6	122.5	122.5	122.6	122.5	122.5	123.4
O18–C17–C19	121.7	122.0	121.9	122.0	122.0	122.0	122.0	118.1
C17–C19–C22	108.8[c]	111.9	111.9	112.0	112.0	112.0	111.9	
RMSD	1.7	1.9	1.8	1.9	1.9	1.9	1.9	
Dihedral angle (°)								
C2–C1–C12–N15	110.4	112.1	111.5	112.0	111.6	112.6	112.5	39.4
C6–C1–C12–N15	−69.1	−67.5	−67.9	−67.5	−67.9	−66.9	−67.0	−141.8
C1–C12–N15–C17	97.0	98.8	97.7	99.5	99.0	99.2	98.8	79.6
C12–N15–C17–O18	4.6	3.1	3.4	3.5	3.5	3.5	3.4	5.6
C12–N15–C17–C19	−175.9	−179.1	−178.2	−178.1	−178.2	−178.2	−178.3	−175.0
RMSD	46.1	47.3	46.9	47.3	47.0	47.7	47.6	

[a] This work.
[b] From Ref [35] for Bis[*N*-benzyl-2-(quinolin-8-yloxy)-acetamide] monohydrate.
[c] C22=H22.

antioxidant activity in these series of N-benzylamides is related to the hydrophobic and hydrophilic regions, these are those regions acceptor or donor hydrogen-bond, as reported for the biological activities that present some sesquiterpenic substances [37–41]. For this reason, in this work those sites in all the series of N-benzylamides were investigated by using the molecular electrostatic potential, atomic charges and bond orders. Table S3 show the molecular electrostatic potential values calculated from the Merz-Kollman (MK) charges [42] for all the N-benzylamides studied. The exhaustive analysis shows clearly that the values for all the atoms practically are not affected by the increase of C atoms in the side chain with exception of the C19 atoms that slightly increase the value from amide (I) to (II). This way, the nucleophilic sites for the series of N-benzylamides are located on the O18 atoms belonging to the C17═O18 groups while the electrophilic sites are positioned on the H16 atoms belonging to the N15—H16 groups, as shown in Fig. S2. Thus, in these N-benzylamides in solid phase are expected hydrogen bonds between two amides molecules in those regions or probably other H bond type in another medium, as observed in the crystal packing of bis[*N*-benzyl-2-(quinolin-8-yloxy)- acetamide] monohydrate [35], O—H···N and N—H···O hydrogen bonds between the acetamide and water molecules.

Examining the MK charges for the series of N-Benzylamides studied at the B3LYP/6-31G* level of theory of Table S4, we observed that the values on the H11 and H16 atoms present slight modifications with the number of C atoms of the side chain while larger changes are observed on the C17, C19 and C22 atoms when increasing the number from 1 up to 2, as can be seen in Fig. S3. Obviously, these variations are attributed to the increase of C atoms in the skeleton of the amides. Also, the MK charges on the O18 and N15 atoms show slight variations with the number of C atoms from 1 to 2. On the contrary, the analysis of the NPA charges summarized in Table S5 doesn't show changes on the atoms of H but on the atoms of C19 and C22 and, also on the N15 and O18 atoms when increasing the length of the side chain from 1 up to 2 and, then it remain practically constant, as observed in Fig. S4.

In this work, the bond orders were expressed as Wiberg indexes and the calculated values are shown in Table S6 while in Fig. S5 are represented graphically the variations with the number of C atoms of the side chain. The analysis for the C atoms show clearly that the values for the C19 and C22 atoms increase quickly with the enlargement of the side chain from 1 up to 2C atoms, a result similar to that observed for the MK and NPA charges while, for the remaining atoms the values are essentially constants, as can be seen in Fig. S6.

4.3. NBO and AIM studies

N-benzylamide compounds such as acetamides have also an excellent coordination ability and high selectivity to metal ions, as reported by Wang et al. [35,43] for two different N-benzylamide complexes. Possibly, those properties are associated to the crystal packing because it is stabilized by hydrogen bonds. In this work, the stabilities of all the series of N-benzylamides were analyzed by using NBO [25,26] and AIM [27,28] calculations. Table S7 show the main delocalization energy values for all the series of N-benzylamides studied at B3LYP/6-31G* level of theory while in Fig. S6 are presented the corresponding stabilization energy values in function of the number of C atoms of the side chain. First, we observed four different delocalizations which are the $\Delta E_{\pi} \rightarrow \pi^{*}$, $\Delta E_{n} \rightarrow \pi^{*}$, $\Delta E_{n} \rightarrow \sigma^{*}$ and $\Delta E_{\pi^{*}} \rightarrow \sigma^{*}$ charges transfer where the latter three have approximately the same energy values, as observed in Fig. S6. Notice that the highest energy values correspond to the $\Delta E_{\pi} \rightarrow \pi^{*}$ delocalizations and, that the energy values for these delocalizations abruptly increase with the number of C atoms from 1 up to 2 and then, the values remain practically constant up to 18C atoms in the side chain. Therefore, the contribution to the total energy, ΔE_{Total}, show a behavior similar to the $\Delta E_{\pi \rightarrow \pi^{*}}$ delocalizations but the ΔE_{Total} values are significantly greater than the $\Delta E_{\pi} \rightarrow \pi^{*}$ delocalizations, as shown Fig. S6. This study shows clearly that the elongation of the side chain stabilizes the series of N-benzylamides studied from the structure (II) up to the structure (VII).

The AIM program [28] was used to investigate the existence of intra-molecular interactions in the different species and to compute their topological properties in gas phase. Thus, Table S8 show the analysis of the bond critical points (BCPs) and ring critical points (RCPs) for the series of N-benzylamides at B3LYP/6-31G* level of theory. According to the Bader's theory [27], the parameters such as the electron density distribution, $\rho(r)$ in the bond critical points (BCPs), the values of the Laplacian, $\nabla^2\rho(r)$, the eigen values $(\lambda 1, \lambda 2, \lambda 3)$ of the Hessian matrix and, the $\lambda 1/\lambda 3$ ratio are of importance to describe the character of interaction between atoms. Thus, when $\lambda 1/\lambda 3 > 1$ and $\nabla^2\rho(r) < 0$ the interaction is typical of covalent bonds (called shared interaction) with high values of $\rho(r)$ and $\nabla^2\rho(r)$ while when $\lambda 1/\lambda 3 < 1$ and $\nabla^2\rho(r) > 0$ the interaction is called closed-shell interaction and is typical of ionic, highly polar covalent and hydrogen bonds as well as of the van-der-Waals and specific intermolecular interactions. This study reveals for all the series of N-benzylamides a BCP represented by the Hydrogen bond interaction (O18…H11) and two RCPs, one associated to the new ring formed and other to the benzyl ring which are named RCP_N and RCP_B, respectively. Fig. S7 show the graphics of the $\rho(r)$, Laplacian and distances related to the O18…H11 interactions and to the RCPs in function of the number of C atoms of the side chain. Note that the representations of the density and Laplacian values remain practically constant with the increase of C atoms in the side chain while only variations in the O18…H11 distances are observed when increasing the carbon skeleton. Here, the low density value in the BCP of N-benzylheptadecanamide could clearly explain the low dipole moment value observed in Fig. S2. This study support the high stabilities of all the series of N-benzylamides studied due to the presence of the intra-molecular O···H interactions (C═O…H—C).

4.4. Frontier orbital and descriptors

For all the series of N-benzylamides, the gap energy values and of some descriptors such as, the chemical potential (μ), electronegativity (χ), global hardness (η), global softness (S) and global electrophilicity index (ω) were calculated from the frontier HOMO and LUMO orbitals at B3LYP/6-31G* level of theory. Note that the HOMO-LUMO gap is calculated as the difference between the calculated HOMO and LUMO energy levels and only provides an approximation to the fundamental gap, as reported by Bredas [44]. This way, Table S9 shows the results for the series of N-benzylamides I—VII studied here while in Fig. S8 are represented the gap values and the descriptors against the number of C atoms in the side chain. In general, the graphic of the gap energy values show a similar behavior for all the series of molecules studied being the most reactive and with less global softness N-benzylpentadecanamide, as observed in Table S9. On the other hand, all the descriptor values remain practically constant when increasing the number of C atoms in the side chain but, according to Table S9; N-benzylpropanamide has the highest global electrophilicity index in agreement with the different MK charges observed on its C atoms (see Fig. S4) and, also with the diminishing of its corresponding electrostatic potential. Thus, this study predicted the following order reactivity for the series of N-benzylamides: (IV) > (VI) > (V) > (VII) > (III) > (II) > (I) indicating clearly that a side chain with a number of C atoms between 14 and 17 is more reactive

than a side chain with a number between 1 and 5. Besides, the tendency observed in the global electrophilicity index is: (II) > (IV) > (V) > (VI) > (III) > (VII) = (I). These results suggest that the highest global electrophilicity index of N-benzylpropilamide (II) is strongly related to the charges and electrostatic potentials values while the higher reactivity and the less global softness that present *N*-benzylpentadecanamide are related to the O···H bonds because the distance O···H increases with the increase of the length of the side chain while decreases the stability.

4.5. Vibrational analysis

The optimized structures of all the members of the N-benzylamides series have C_1 symmetries and, for this reason, all their vibrations are IR and Raman active. In this analysis, due to the high number of vibration normal modes of N-Benzylhexadecanamide (V), N-Benzylheptadecanamide (VI) and N-Benzyloctadecanamide (VII) (186, 195 and 204, respectively) the SQM methodology [30] was employed only for N-benzylacetamide (I) which has 60 vibration normal modes; N-Benzylhexanamide (III) with 90 vibration normal modes and, N-benzylpentadecanamide (IV) with 177 vibration normal modes. Fig. 3 show a comparison among the available experimental infrared spectra of (I) taken from Ref. [45] and those corresponding to benzylamides (IV), (V), (VI) and (VII) while the theoretical infrared spectra for all the members of this series from (I) to (VII) calculated at the B3LYP/6-31G* level in gas phase can be seen in Fig. 4. The latter figure show clearly that the bands located between 3200 and 2900 cm^{-1}, which are associated to the stretching modes of the CH_2 groups, increase significantly their intensities when the quantity of those groups in the side chain increase from (I) to (VII) while in the lower wavenumbers region diverse changes are observed. Hence, we observed that the most intense bands in the IR spectrum of (I) at 1713 and 1611 cm^{-1} have a intensity *R* relationship of 1.34 while theoretically both bands are predicted at 1772 and 1556 cm^{-1}, respectively with inverted intensities from (II) up to (VII) and with a relationship between them of 1.15, as observed in Fig. 4. Fig. 5 shows these two bands clearly identified in the experimental and theoretical IR spectra of (I) together with the *R* relationship and with the assignments of the principal bands. On the other hand, the calculated relationship between those two bands for (II) is 1.29, for (III) is 1.09, for (IV) is 1.25, for (V) is 1.22, for (VI) is 1.25 and for (VII) is 1.21. This way, the graphic of the calculated *R* relationships for all the members series in function of the number of C atoms in the side chain from (I) to (VII) are practically constant while the experimental behaviors of the derivatives from (IV) to (VII) are completely different because the *R* value for (IV) is similar to (V) but different from those corresponding to (VI) and (VII), as can be seen in Fig. S9. On the other hand, when Figs. 3 and 4 were carefully compared, we observed that in the calculated IR spectra for all the compounds of the series those two intense bands, associated with the C═O stretching and N—H bending modes, respectively, do not present changes in their intensities from (I) up to (VII) while in the experimental spectra

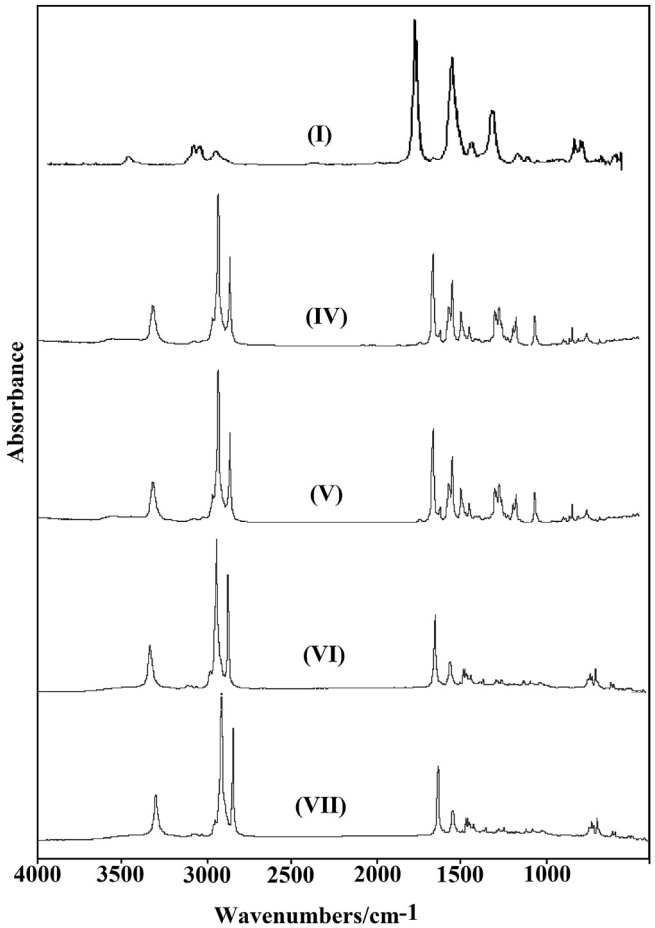

Fig. 3. Comparison between the experimental infrared spectra of N-benzylacetamide (I) in solid phase from Ref. [45] with those corresponding to N-benzylpentadecanamide (IV), N-benzylhexadecanamide (V), N-benzylheptadecanamide (VI) and N-benzyloctadecanamide (VII).

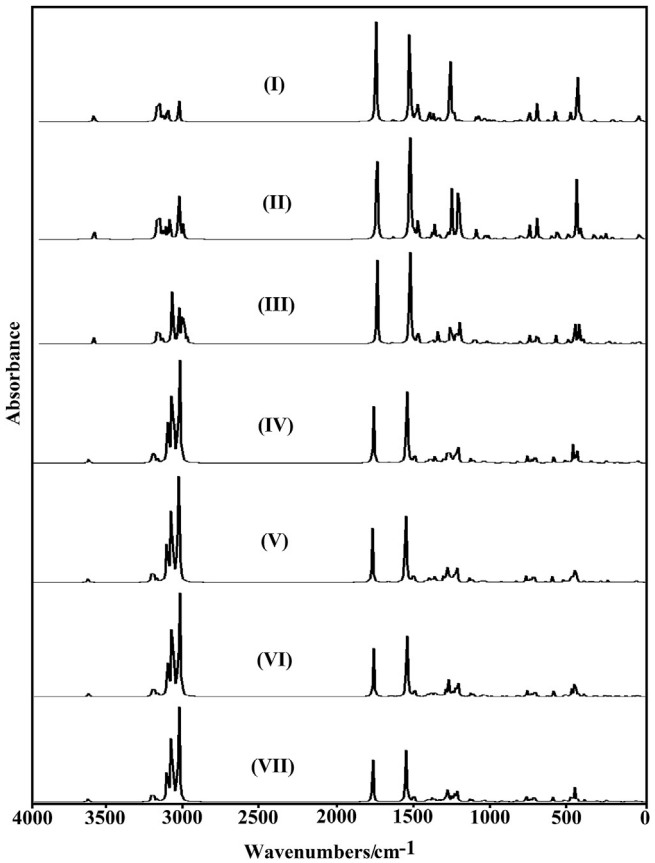

Fig. 4. Comparison between the theoretical infrared spectra of N-benzylacetamide (I), *N*-benzylpropilamide (II), *N*-benzyl hexanamide (III), *N*-benzylpentadecanamide (IV), N-benzylhexadecanamide (V), N-benzylheptadecanamide (VI) and N-benzyloctadecanamide (VII) in gas phase at B3LYP/6-31G* level of theory.

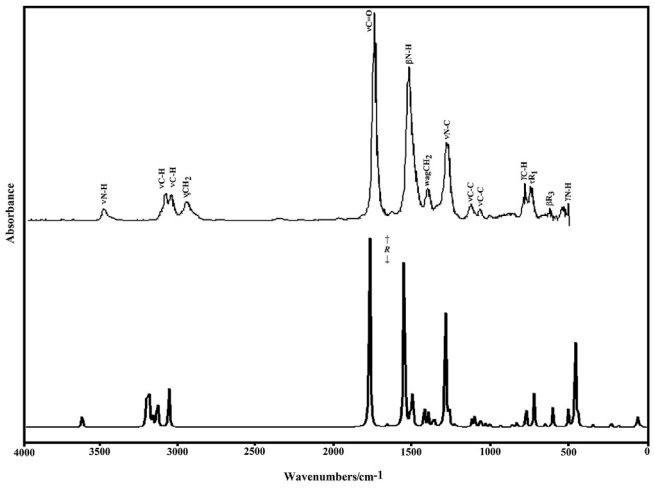

Fig. 5. Comparison between the experimental infrared spectra of N-benzylacetamide (I) (upper) in solid phase from Ref. [45] with the corresponding theoretical (bottom) by using 6-31G* basis set.

significant changes are observed in the intensities of those two bands. Moreover, in all species the higher intensities were observed in the vibration modes associated with the CH_2 group linked to benzyl and NH groups, indicating that the number of CH_2 groups in the side chain only have influence on the stretching modes (higher wavenumbers region) than on the other ones (lower wavenumbers region). Thus, the interactions due to increasing of C atoms in the side chain and the existence of inter-molecular N—H…O bonds, not considered in the theoretical calculations, could in part justify the differences observed between the experimental and theoretical spectra in the lower wavenumbers region. Another possible reason of the constant intensity of the band associated to the C═O groups could be related to the O…H interactions because these H bonds stabilize the C═O bonds, as revealed by the AIM analysis. The observed IR and Raman bands for (I), (IV) and (VII) are presented in Table 2 together with the SQM frequencies for (I), (III) and (IV) and the proposed assignments for the seven species studied. It is necessary to clarify that the assignments for these three (I), (III) and (IV) derivatives were performed using the SQMFF methodology [30], the Molvib program [31] and considering the calculated PED contributions between 10 and 7% at the B3LYP/6-31G* level of theory while the assignments for the (V), (VI) and (VII) species were performed at the same level of theory and with the aid of the *GaussView* program [32]. This way, all the experimental and calculated frequencies can be seen in Table S10. The Rauhut and Pulay transferable scale factors [30] were employed to calculate the force fields of (I), (III) and (IV) using the B3LYP/6-31G* level of theory. The discussions of the assignments of some groups are presented below.

4.5.1. Band assignments

4.5.1.1. NH modes. In compounds containing this group, the NH stretching modes are assigned between 3480 and 3254 cm^{-1} [2,3,46], hence, for (I) the IR band at 3477 cm^{-1} is assigned to this mode but in the species from (IV) to (VII) the band attributed to these modes are observed shifted and with higher intensities, as can be seen in Fig. 3. Thus, those modes for the four latter derivatives are clearly assigned to the band at 3309 cm^{-1}. Note that the shifting of those bands are probably justified by the existence of inter-molecular N—H…O bonds, as experimentally reported for N-benzylacetamide by Smiszek-Lindert and Kusz [36] while the increasing in their intensities are related to the quantity of CH_2 groups in the side chain. The corresponding deformation mode for (I) is predicted at 1483 cm^{-1}, for (III) and (IV) are predicted at 1507 cm^{-1} while for the remaining species are predicted at 1554 cm^{-1}. The out-of-plane deformation or torsion NH modes for all the members of the series are predicted at different wavenumbers, thus, for (I) is predicted at 455 cm^{-1}, for (III) at 470 cm^{-1} and for (IV) at 468 cm^{-1} while for the remaining members are predicted at 525 cm^{-1}, therefore, these modes are assigned in accordance with the calculations.

4.5.1.2. CH modes. The C—H stretching modes for all the N-benzyl derivatives are predicted by the SQM calculations at the B3LYP/6-31G* level of theory in the expected regions [2–4,40,41] and coupled among them, for this reason, they are easily assigned to the IR and Raman bands between 3216 and 3041 cm^{-1}, as indicated in Table 2. The calculated SQM predicted the in-phase modes between 1500 and 1100 cm^{-1} while between 1000 and 700 cm^{-1} are predicted the corresponding out-of-phase modes, as observed in Table 2. Thus, both modes were assigned accordingly.

4.5.1.3. CH_3 modes. For the (I), (III) and (IV) N-benzyl derivatives the nine expected vibration modes corresponding to this group are predicted by SQM calculations as pure modes while for the remaining species the *GaussView* program [30] identify quickly the positions of these modes, hence, they were easily assigned, as observed in Table 2. Note that the antisymmetric and symmetric stretching modes are observed in different regions, thus, these modes for (V), (VI) and (VII) are predicted at the same wavenumbers while for (III) and (IV) the wavenumbers are different from (I). Similar behaviors are observed in the antisymmetric and symmetric CH_3 deformation modes. Hence, we observed that in general all the modes corresponding to this group are highly influenced by the quantity of C atoms in the side chain, for example, the rocking and twisting modes for (V), (VI) and (VII) are predicted at higher wavenumbers than the (I), (III) and (IV) species, as shown in Table 2.

4.5.1.4. CH_2 modes. The vibration modes related with these groups in all the species were predicted in the expected regions [1,3,4,40,41], as can be seen in Table 2. Obviously, the increasing of C atoms from (I) up to (VII) increase the intensities of the bands related to this group, especially those bands associated to the stretching modes, as can be seen in Figs. 3 and 4. Note that Fig. 5 show a very good agreement between both IR spectra while, as explained above, for the other species there are differences between the corresponding spectra due to that the predicted bands associated to the NH bending modes do not show changes in their intensities while in the experimental spectra a slightly decreasing is observed.

4.5.1.5. CO modes. For the (I), (III) and (IV) species the SQM calculations clearly predicted the C═O stretching modes between 1713 and 1705 cm^{-1} with approximately the same intensities while, for (V), (VI) and (VII), the B3LYP/6-31G* method predicted these modes at 1769 cm^{-1}. Here, the increasing of C atoms in the side chain do not affect the intensities of these bands probably because the O atoms of these groups are forming H bonds that stabilize the C═O bonds, as revealed by the AIM analysis. The bending, wagging, rocking and twisting modes related to these groups for all the species are predicted in the expected regions [1,40,41].

4.5.1.6. Skeletal modes. The B3LYP/6-31G* calculations predicted the C═C stretching modes belonging to the benzyl rings of all the members of the series in the same regions and, as reported in similar molecules [1–4,40,41,46], for these reasons, they were

Table 2
Observed and calculated wavenumbers (cm^{-1}) and assignment for the series of N-benzylamides studied.

I	IV[a]		VII[a]		I[a]		III[a]		IV[a]		V, VI, VII[a,e]	
IR[b] Acetamide	IR[a]	Raman[a]	IR[a]	Raman[a]	SQM[c]	Assignment[a]	SQM[c]	Assignment[a]	SQM[c]	Assignment[a]	Calc[d]	Assignment[a]
3477w	3309 m		3309 m		3456	νN15-H16	3471	νN15-H16	3469	νN15-H16	3619	νN15-H16
		3296vw		3216vw							3209	νC-H
											3202	νC-H
		3130vw	3128w	3127w							3192	νC-H
3076w	3073 w	3077vw	3083w		3077	νC4-H9	3077	νC4-H9	3077	νC4-H9	3183	νC-H
			3068w		3070	νC6-H11	3070	νC6-H11	3069	νC6-H11	3171	νC-H
				3057w	3060	νC3-H8	3060	νC3-H8	3060	νC3-H8	3133	ν_aCH_2
					3051	νC5-H10	3051	νC5-H10	3051	νC5-H10	3110	ν_aCH_3
3041w		3020 vw	3037w		3039	νC2-H7	3039	νC2-H7	3039	νC2-H7	3106	ν_aCH_3
	3013w			3010vw	3016	ν_aCH_3					3103	ν_aCH_2
		3007 vw			3006	ν_aCH_3					3079	ν_aCH_2
					3004	ν_aCH_2(C12)	3004	ν_aCH_2(C12)	3004	ν_aCH_2(C12)		
							2983	ν_aCH_3	2981	ν_aCH_3		
							2978	ν_aCH_3	2977	ν_aCH_3		
			2963sh	2966vw			2974	ν_aCH_2(C22)	2975	ν_aCH_2(C22)	3075	ν_aCH_2
	2953w		2955w						2951	ν_aCH_2(C40)	3070	ν_aCH_2
									2946	ν_aCH_2(C49)		
					2940	ν_sCH_2(C12)	2941	ν_aCH_2(C19)	2940	ν_aCH_2(C19)	3067	ν_aCH_2
2939w					2938	ν_sCH_3	2939	ν_sCH_2(C12)	2940	ν_aCH_2(C52)	3065	ν_sCH_2
							2937	ν_aCH_2(C28)	2937	ν_sCH_2(C12)	3065	ν_aCH_2
		2932vw		2928w					2933	ν_aCH_2(C55)	3059	ν_aCH_2
									2926	ν_aCH_2(C34)	3052	ν_aCH_2
			2918vs				2917	ν_sCH_2(C22)	2919	ν_aCH_2(C43)	3046	ν_aCH_2
	2919vs								2915	ν_sCH_2(C22)	3042	ν_sCH_3
							2916	ν_sCH_3	2915	ν_sCH_3	3039	ν_aCH_2
2908sh							2909	ν_aCH_2(C25)	2911	ν_aCH_2(C31)	3036	ν_aCH_2
									2908	ν_aCH_2(C25)	3033	ν_aCH_2
									2907	ν_aCH_2(C28)	3032	ν_aCH_2
									2906	ν_aCH_2(C46)	3030	ν_aCH_2
			2908sh				2905	ν_sCH_2(C19)	2906	ν_aCH_2(C37)	3029	ν_sCH_2
									2904	ν_sCH_2(C55)	3029	ν_sCH_2
									2904	ν_sCH_2(C19)	3027	ν_sCH_2
							2902	ν_sCH_2(C28)	2902	ν_sCH_2(C34)	3025	ν_sCH_2
	2867sh	2884w		2882 m			2886	ν_sCH_2(C25)	2898	ν_sCH_2(C46)	3021	ν_sCH_2
									2894	ν_sCH_2(C28)	3017	ν_sCH_2
									2890	ν_sCH_2(C43)	3014	ν_sCH_2
									2889	ν_sCH_2(C40)	3014	ν_sCH_2
									2887	ν_sCH_2(C49)	3012	ν_sCH_2
									2886	ν_sCH_2(C52)	3011	ν_sCH_2
			2873w						2885	ν_sCH_2(C37)	3011	ν_sCH_2
										ν_sCH_2(C52)		
									2885	ν_sCH_2(C25)	3009	ν_sCH_2
	2850s	2849w	2850s	2849w					2884	ν_sCH_2(C31)	3008	ν_sCH_2
1719vs	1714w				1713	νC17═O18	1704	νC17═O18	1705	νC17═O18	1769	νC17═O18
	1636s	1645w	1638s	1633w							1665	νC═C
1603w	1608w	1613w	1605w	1604w	1611	νC5-C6	1611	νC5-C6	1611	νC5-C6	1645	νC═C
	1593w	1596w	1551m	1585w	1591	νC6-C1	1591	νC1-C2	1591	νC3-C4	1554	βN15-H16
										νC1-C2		
	1542w										1541	δCH_2
											1530	δ_aCH_3
	1522m	1518w	1517sh				1507	βN15-H16	1507	βN15-H16	1526	δ_aCH_3
1498s	1505sh				1500	βC5-H10	1498	βC6-H11	1498	βC5-H10	1498	δCH_2
						νC4-C5				βC2-H7		
			1493w	1492sh	1483	βN15-H16	1475	δ_aCH_3	1476	δCH_2(C46)		
									1474	δCH_2(C28)		
			1473w						1471	δ_aCH_3		
	1469w						1466	δCH_2(C22)	1467	δCH_2(C22)		
							1465	δ_aCH_3	1465	δ_aCH_3		
		1460vs	1462w	1461m					1462	δCH_2(C31)		
1459sh					1458	βC3-H8	1458	βC4-H9	1458	βC3-H8		
	1457sh								1457	δCH_2(C37)		
			1454w		1452	δ_aCH_3	1454	δCH_2(C28)	1453	δCH_2(C55)		
									1449	δCH_2(C25)	1442	δ_aCH_3
							1449	δCH_2(C25)	1449	δCH_2(C43)		
1447sh									1447	δCH_2(C49)		
									1446	δCH_2(C52)		
									1444	δCH_2(C34)		
	1442w	1440vs	1442w	1441s					1444	δCH_2(C40)		
					1437	δ_aCH_3			1437	δCH_2(C12)	1428	$wagCH_2$
					1435	δCH_2	1435	δCH_2(C12)			1427	$wagCH_2$
	1420w	1426sh	1428w	1418w			1433	δCH_2(C19)	1431	δCH_2(C19)	1426	$wagCH_2$

(*continued on next page*)

Table 2 (*continued*)

I	IV[a]		VII[a]		I[a]		III[a]		IV[a]		V, VI, VII[a,e]	
IR[b] Acetamide	IR[a]	Raman[a]	IR[a]	Raman[a]	SQM[c]	Assignment[a]	SQM[c]	Assignment[a]	SQM[c]	Assignment[a]	Calc[d]	Assignment[a]
									1407	$wagCH_2$(C40)	1425	$wagCH_2$
									1406	$wagCH_2$(C43)	1424	$wagCH_2$
							1404	$wagCH_2$(C25)	1403	$wagCH_2$(C25) $wagCH_2$(C49)	1419	$wagCH_2$
									1402	$wagCH_2$(C31) $wagCH_2$(C28)	1411	$wagCH_2$
		1390w	1394w				1391	$wagCH_2$(C28)	1398	$wagCH_2$(C52)	1403	$wagCH_2$
									1388	$wagCH_2$(C55)	1396	$wagCH_2$
1375w	1383w			1374w	1380	$wagCH_2$	1382	$wagCH_2$(C12)	1381	$wagCH_2$(C12)	1380	$wagCH_2$
			1376w				1377	$\delta_s CH_3$	1377	$\delta_s CH_3$	1370	βC-H
	1362w	1361w	1357w		1362	$\delta_s CH_3$			1368	$wagCH_2$(C19)	1364	βC-H
							1343	$wagCH_2$(C19)	1349	$wagCH_2$(C34)	1360	ρCH_2
	1331vw		1333w		1337	βC6-H11	1336	βC2-H7	1337	βC6-H11	1342	ρCH_2
		1327w							1326	$wagCH_2$(C46)	1334	ρCH_2
	1320vw		1320w						1319	ρCH_2(C46)	1327	ρCH_2
									1318	ρCH_2(C40) ρCH_2(C31)	1316	ρCH_2
1315vw			1312w		1314	νC1-C2	1314	νC3-C4	1314	νC4-C5		
									1313	ρCH_2(C34) ρCH_2(C25)		
	1310vw						1310	ρCH_2(C28)	1312	ρCH_2(C28) ρCH_2(C49)		
									1308	ρCH_2(C52)	1310	ρCH_2
							1306	ρCH_2(C22)	1305	ρCH_2(C37)		
									1301	ρCH_2(C43)	1296	ρCH_2
		1296m	1290w	1296s					1293	ρCH_2(C22)	1292	ρCH_2
	1288vw		1282w						1281	ρCH_2(C55)	1280	ρCH_2
	1267w	1267w	1274w				1272	ρCH_2(C25)	1269	$wagCH_2$(C22)	1274	ρCH_2
	1257w		1262w				1253	$wagCH_2$(C22)	1256	ρCH_2(C19)	1269	ρCH_2
1246m			1249w	1248w	1246	ρCH_2			1244	ρCH_2(C12)	1255	$wagCH_2$
	1239w		1234w				1239	ρCH_2(C12)	1237	ρCH_2(C12)	1237	$wagCH_2$
1230sh	1227w	1225w	1221w		1224	νN15-C17			1228	ρCH_2(C19)	1231	$wagCH_2$
									1215	$wagCH_2$(C37)	1228	$wagCH_2$
	1209w		1206w	1205w			1206	νN15-C17	1202	νN15-C17	1214	βC-H
		1199w	1189w		1192	C1-C12	1192	νC1-C12	1192	νC1-C12	1193	βC-H
	1189w	1184vw			1180	βC2-H7	1180	βC5-H10	1181	νN15-C17		
			1177 w	1175 w					1179	βC5-H10 βC3-H8		
			1165w		1160	βC4-H9	1160	ρCH_2(C19)	1160	βC4-H9		
1152vw	1157w	1157vw					1159	βC3-H8	1150	ρCH_2(C19)	1153	ρCH_3
	1139w	1131m	1130sh	1130m					1130	ρCH_3	1136	ρCH_2
	1116vw	1108w	1119w	1116sh			1117	ρCH_3	1113	ρCH_2(C19)	1118	βC-H
			1094sh						1094	ρCH_3	1092	νC-N
1089w			1082w		1080	C2-C3	1080	νC2-C3	1080	νC2-C3		
		1063m	1066w	1063s			1071	$\rho' CH_3$	1074	νC12-N15	1078	νC-C
					1046	C12-N15			1053	νC19-C22	1074	νC-C
					1040	ρCH_3	1040	νC12-N15	1038	νC52-C55	1040	νC-C
									1035	νC43-C46	1037	νC-C
							1034	νC25-C28	1034	νC37-C40 νC34-C37		
		1032w							1032	νC25-C28		
1030vw									1031	νC22-C25	1028	νC-C
	1027w		1028w	1027w	1027	νC3-C4	1027	νC4-C5	1026	βR_1, νC3-C4	1018	βR_1
			1020w						1023	νC19-C22		
									1017	νC12-N15	1013	νC-C
	1000sh	1009w		1004s			1008	νC19-C22	1006	νC55-C58	1008	νC-C
					998	βR_1	998	βR_1	998	βR_1	1006	νC-C
		996vw	996w		996	γC5-H10	995	γC6-H11	994	γC6-H11	1001	γC-H
990vw									990	νC46-C49	987	νC-C
			985w				987	νC22-C25	987	γC5-H10 γC4-H9	984	νC-C
			974w		980	C17-C19	982	τwCH_2(C12)	977	νC49-C52	975	γC-H
971vw	972vw								970	$\rho' CH_3$		
		964w			967	γC3-H8	966	γC3-H8	965	γC3-H8		
959vw					955	$\rho' CH_3$			955	νC28-C31	974	γC-H
	952vw		947w	951vw					953	νC40-C43 νC31-C34	935	νC-C
	924vw			930vw			926	τwCH_2(C22)	922	γC2-H7	931	γC-H
909vw		917w		910vw	918	γC2-H7	918	γC2-H7	918	γC4-H9	905	$\rho' CH_3$
		896w	871w	892w			886	νC28-C31	876	ρCH_3 νC52-C55	884	τwCH_2
		860vw							869	τwCH_2(C40)	867	γC-H
857vw	857w			854w	858	γC6-H11	857	γC5-H10	856	γC5-H10	856	τwCH_2

Table 2 (*continued*)

I	IV[a]		VII[a]		I[a]		III[a]		IV[a]		V, VI, VII[a,e]	
IR[b] Acetamide	IR[a]	Raman[a]	IR[a]	Raman[a]	SQM[c]	Assignment[a]	SQM[c]	Assignment[a]	SQM[c]	Assignment[a]	Calc[d]	Assignment[a]
	843w		840w	839sh			829	νC17-C19	835	τwCH$_2$(C12) νC17-C19	830	νC-C
	819w		819w	818w					820	τwCH$_2$(C19)	823	τwCH$_2$
806vw	803w	807vw		800sh	810	δC1C12N15	810	δC1C12N15 νC6-C1	809	δC1C12N15 νC6-C1	794	τwCH$_2$
794vw					799	τw CH$_2$	797	τwCH$_2$(C19)			771	γC-H
	767w	771 m	775w	774sh					775	τwCH$_2$(C25)	769	γC-H
751w			760w		756	γC4-H9	757	γC4-H9	756	τR$_1$, γC4-H9	754	τwCH$_2$
	749w	747w	746w	748w					736	τwCH$_2$(C55)	745	τwCH$_2$
	719w	729vw	731w				717	γC17═O18	710	γC17═O18	719	γC-H
703w			719w		701	τR$_1$, γC3-H8	702	τR$_1$, γC3-H8	701	τR$_1$, γC3-H8		
			698w	699vw			690	τwCH$_2$(C28) βC17═O18	696	βC17═O18		
			686w						679	τwCH$_2$(C37)		
									667	τwCH$_2$(C22) τwCH$_2$(C34)		
	666vw		666sh				663	τwCH$_2$(C25)	662	τwCH$_2$(C52) τwCH$_2$(C49)		
									660	τwCH$_2$(C31) τwCH$_2$(C28)	646	τwCH$_2$
					632	βR$_2$			660	τwCH$_2$(C43) τwCH$_2$(C46)		
	639vw	640w	636w		626	γC17═O18	632	βR$_2$	632	βR$_2$	635	βR$_2$
612w	618sh		609w	619w	598	βC17═O18	625	τR$_1$	624	τR$_1$		
589w	598vw	598w	594w	594sh	590	τR$_1$					598	τR$_1$
583w	587vw	575w	573sh				588	βR$_3$	588	βR$_3$		
		552w									526	γN-H
	519vw		511w	514vw					518	βR$_3$	517	δCCC
			497w				509	τR$_2$	507	δC28C31C34 δC37C40C43	510	δCCC
491w	493vw	484vw	489w	482vw	493	βR$_3$			498	τR$_2$	478	δCCC
460w	470vw	463vw	469w	470vw			470	γN15-H16	468	γN15-H16	474	δCCC
	452vw		449w		455	γN15-H16			448	δC49C52C55 δC31C28C25	455	δCCC
	440vw	439vw		440vw			439	γN15-H16 τR$_2$	441	γN15-H16 τR$_2$	438	δCCC
	434vw		433w		431	τR$_2$						
	416vw		419w	419vw			416	δC31C28C25	414	τR$_2$	418	τR$_2$
	405vw	400w	407sh		404	τR$_3$	404	τR$_3$	404	τR$_3$	410	δCCC
		379 m					368	δC25C22C19	367	δC52C55C58 δC25C22C19	391	δCCC
				338vw	338	βC1-C12 δN15C17C19			349	βC1-C12	349	δCCC
				310vw			317	βC1-C12	316	βC1-C12 τR$_2$	327	βC-C
		280vw		288sh	290	τR$_2$ δC1C12N15			296	τR$_2$ δC1C12N15	308	δCCC
				267sh			258	δC22C25C28	252	δC17C19C22	289	δCNC
							241	δN15C17C19	238	δC43C46C49	251	τwCH$_3$
				226sh					228	τwCH$_3$	249	δCCC
		215vw					224	τwCH$_3$	216	δC12N15C17 δN15C17C19 δC40C43C46	220	δCCN
		188w		187w			206	δC12N15C17			187	γC-C
					167	τC1-C6	167	τC1-C6-	177	γC1-C12	175	τC-C
				162sh					157	τC43-C40	173	τC-C
									156	τC40-C37	161	τC-C
				154sh					154	τC34-C31	155	τC-C
		139sh							139	τC49-C46 τC31-C28	143	τC-C
				133 sh			129	τC28-C25	134	τC46-C43	133	τC-C
				120sh					122	δC34C37C40	122	τC-C
		112sh							114	τC55-C52	118	τC-C
									107	τC25-C22 τC37-C34	106	τC-C
				101vs			102	τC25-C22	100	δC46C49C52 δC31C34C37	103	τC-C
		92sh					95	δC17C19C22	84	τC22-C19	91	τC-C
					67	τwC17-N15			77	τC52-C49	80	τC-C
							57	τC22-C19	61	τwC17-N15 γN15-H16	72	τC-C
					52	τC12-N15			53	τC19-C17	55	τC-C

(*continued on next page*)

Table 2 (*continued*)

I	IV[a]		VII[a]		I[a]		III[a]		IV[a]		V, VI, VII[a,e]	
IR[b] Acetamide	IR[a]	Raman[a]	IR[a]	Raman[a]	SQM[c]	Assignment[a]	SQM[c]	Assignment[a]	SQM[c]	Assignment[a]	Calc[d]	Assignment[a]
							50	τwC17-N15	51	δC22C25C28	49	τC-C
					42	τwCH$_3$	43	τC12-N15	44	τC12-N15	44	τC-C
									36	τwC17-N15	38	τC-C
					29	τwC1-C12			27	τC28-C25	31	τC-C
							26	τC1-C12	25	τC1-C12	22	τC-C
									17	τwC17-N15 τC1-C12	14	τC-C
							13	τC19-C17	15	τwC17-N15	9	τwC-N
									8	τC19-C17	5	τC-C

[a] This work.
[b] From Ref. [45].
[c] From scaled quantum mechanics force field.
[d] Calculated by DFT B3LYP/6-31G*.
[e] Assigned by *GaussView* program [32].

assigned accordingly, as presented in Table 2. On the other hand, the C–C stretching modes belonging to the side chain are also predicted for all the species between 1192 and 829 cm^{-1}. The deformation and torsion ring modes for (I), (III) and (IV) are predicted by SQM calculations in the expected regions [2,4,46], hence they were clearly assigned, as observed in Table 2. The remaining skeletal modes were assigned and can be seen in Table 2.

5. Force field

The SQM methodology [30] and the Molvib program [31] were used to calculate the scaled force fields for the (I), (III) and (IV) species at the B3LYP/6-31G* level of theory. Then, the force constants expressed by means of internal coordinates were also calculated at the same level of theory and, afterward compared in Table 3 with those reported for compounds containing similar groups such as, the most stable conformer of thymidine [3] and the 2-[[5-amino-5-oxo-2-(phenylmethoxycarbonylamino) pentanoyl] amino] acetic acid [47]. In general, the values for the three N-benzylamide species show good concordance with those reported for thymidine and APPA [3,47] and, the differences observed in the *f(νC=O)* and *f(νC=C)* force constants of the three derivatives in relation to thymidine and APPA, respectively are evidently attributed, in the first case to a higher number of C=O groups while in the second one, to the C=C distances of thymidine because it has a pyrimidine ring instead benzyl, as in our case. Comparing the force constants for the three N-benzylamides species, it is observed higher differences in the *f(νCH$_2$)* and *f(νCH$_3$)* force constant values, a similar result to that observed in the stretching modes corresponding to the CH$_2$ and CH$_3$ groups. Thus, in the Section 4.5.1.3., we observed that all the modes corresponding to the CH$_3$ group are highly influenced by the quantity of C atoms in the side chain decreasing the frequencies related to the stretching modes from (I) to (VII), in accordance to those force constants. For (I), it is N-benzylacetamide, the *f(νCH$_2$)* force constant is slightly higher while for the remaining derivatives the values decrease in agreement to the stretching CH$_2$ modes which are influenced by the longitude of C atoms in the side chain, as observed from the vibrational analysis. The behavior of the *f(νCH$_2$)* force constant in function of the number of C atoms in the side chain is logarithmic, with a very good correlation coefficient of 0.9959, thus, the *f(νCH$_2$)* force constants for (V) and (VII) can be easily calculated from the corresponding equation, as can be seen in Fig. S10.

Table 3
Comparison of scaled internal force constants for the series of seven N-benzylamides studied. Units are mdyn Å^{-1} for stretching and stretching/stretching interaction and mdyn Å rad^{-2} for angle deformations.

B3LYP/6-31G*[a]					
Force constant	(I)	(III)	(IV)	C3[b]	APPA[c]
f(νN-H)	6.68	6.68	6.68	6.63	6.56
f(νC-H)	5.14	5.14	5.14	5.22	5.15
f(νC=O)	11.43	11.31	11.33	11.63	11.92
f(νC=C)	6.50	6.50	6.50	8.17	6.51
f(νC$_B$-CH$_2$)	4.19	4.19	4.19		
f(νCH$_2$)	4.87	4.75	4.69		4.91
f(νCH$_3$)	4.92	4.83	4.83		
f(δCH$_2$)	0.77	0.78	0.79	0.77	0.77
f(δCH$_3$)	0.54	0.56	0.56		

[a] This work.
[b] From Ref [3] for thymidine.
[c] From Ref [47] for APPA: 2-[[5-amino-5-oxo-2-(phenylmethoxycarbonylamino) pentanoyl] amino] acetic acid.

6. Ultraviolet–visible spectrum

The electronic spectra of N-benzylacetamide in a methanol (MeOH) solution taken from Ref. [45] compared to the calculated spectra of all the *N*-benzylacetamides series at the B3LYP/6-31G* level are observed in Fig. S11 while in Table 4 are summarized the positions of the bands, their corresponding energies and the oscillator strengths, f. The experimental spectrum of (I) show two intense and broad bands at 242 and 202 nm while the theoretical bands for all the series members are predicted in the 218–205 nm and 173–162 nm regions, respectively. In the UV spectrum of benzene in hexane solution two bands are reported around 254 and 204 nm for non-conjugated derivatives where the first band is shifted to lower wavelengths when some substituent is conjugated to the aromatic system, as in (I), whose band is observed at 242 nm. Both bands are easily attributed to $\pi \rightarrow \pi^*$ transitions due to the presence of C=C double bonds, as reported in the literature [48,49]. Here, we observed that the increasing of C atoms in the side chain produce the shifting of the most intense band toward lower wavelengths and, in addition, the intensities increasing in all cases, as shown Fig. S11.

7. NMR study

Table S11 and S12 show a comparison between the experimental and calculated chemical shifts for the H and C atoms, respectively. The calculated chemical shifts of the ^{1}H and ^{13}C NMR for all the N-benzylamides studied were obtained by using the GIAO method [34] and the B3LYP/6-31G* level of theory.

Table 4
TD-DFT calculated visible absorption wavelengths (nm) and oscillator strengths (f) for all the series of N-benzylamides studied.

B3LYP6-31G*[a]				Experimental[b]		B3LYP6-31G*[a]			Experimental[b]	
Species	Energy Transition[a] (eV)	λ (nm)	f	λ (nm)	Assignment[a]	Energy transition[a] (eV)	λ (nm)	f	λ (nm)	Assignment[a]
(I)	5.6766	218.41	0.0003	242	π → π*(C=C)	7.1407	173.63	0.5140	202	π → π*(C=C)
(II)	6.0004	206.63	0.0517			7.2181	171.77	0.4142		
(III)	6.0266	205.73	0.0126			7.7395	160.20	0.6585		
(IV)	6.0269	205.72	0.0129			7.6435	162.21	0.8174		
(V)	6.0269	205.72	0.0129			7.6432	162.22	0.8149		
(VI)	6.0268	205.72	0.0127			7.6436	162.21	0.8145		
(VII)	6.0269	205.72	0.0129			7.6432	162.22	0.8148		

[a] This work.
[b] Ref. [48,49].

Experimentally, the ^{1}H NMR spectrum of (I) shows the chemical shifts for the H atoms corresponding to: (i) the benzyl ring in the range of δ (7.47–7.04) ppm, (ii) the NH bond at 6.4 ppm, (iii) the CH_2 group at 4.35 ppm and, (iv) the CH_3 group at 1.94 ppm. This way, the calculated chemical shifts for the H atom show a reasonable agreement with the experimental values with observed RMSD value between 0.66 and 0.61 ppm, while the chemical shifts for the carbon atoms show a higher RMSD value (1.08 and 0.85 ppm). The experimental and calculated chemical shifts for both H and C atoms are in satisfactory agreement taking into account that they were calculated by using 6-31G* basis set. In this case, due to the high number of C atoms in the side chains of (IV), (V), (VI) and (VII) was impossible to compute the 6–311++G** calculations to predict chemical shifts soundly. For these reasons, ONION calculations were employed.

8. Conclusions

In the present work, we have characterized four members of the N-benzylamides series isolated from Maca (*Lepidium meyenii*), i.e., N-benzylpentadecanamide, N-benzylhexadecanamide, N-benzylheptadecanamide and N-benzyloctadecanamide by using FTIR, FT-Raman and ^{1}H and ^{13}C NMR spectroscopies. Their molecular structures in gas phase were determined by using B3LYP/6-31G*/ONION calculations. Here, the atomic charges, molecular electrostatic potentials, stabilization energies, topological properties of those macamides were analyzed as a function of the number of C atoms of the side chain. Here, the properties of the four macamides were compared with those also calculated in this work for the N-benzylacetamide, N-benzylpropanamide and N-benzylhexanamide derivatives. The NBO and AIM calculations reveals the high stabilities of all the N-benzylamides series studied due to the presence of the intra-molecular O···H interactions (C=O…H–C). The HOMO-LUMO study predicted the following order reactivity: (IV) > (VI) > (V) > (VII) > (III) > (II) > (I) and suggest clearly that a side chain with a number of C atoms between 14 and 17 is more reactive than a side chain with a number between 1 and 5. Besides, the order observed in the global electrophilicity index of N-benzylpropanamide (II) is strongly related to the charges and electrostatic potentials values while the higher reactivity and the less global softness that present N-benzylpentadecanamide are related to the O···H bonds because the distance O···H increases with the increase of the side chain length while decreases the stability. The force fields and the complete vibrational assignments were only reported for N-benzylacetamide, N-benzylhexanamide and N-benzylpentadecanamide due to the large number of vibration normal modes that present the macamides with longer side chain. Thus, a complete assignment of the 177 normal vibration modes of the N-benzylpentadecanamide was performed taking into account the SQM force field employing the B3LYP/6-31G* combination. The calculated force constant values are in accordance with the values reported for similar molecules.

Acknowledgments

This work was supported with grants from CIUNT (Consejo de Investigaciones, Universidad Nacional de Tucumán) and CONICET (Consejo Nacional de Investigaciones Científicas y Técnicas, R. Argentina). The authors would like to thank Prof. Tom Sundius for his permission to use MOLVIB.

Appendix A. Supplementary data

Supplementary data related to this article can be found at http://dx.doi.org/10.1016/j.molstruc.2015.10.082.

References

[1] F.E. Chain, P. Leyton, C. Paipa, M. Fortuna, S.A. Brandán, Spectrochim. Acta Part A 138 (2015) 303–313.
[2] M.J. Márquez, M.B. Márquez, P.G. Cataldo, S.A. Brandán, Open J. Synthesis Theory Appl. 4 (2015) 1–19.
[3] M.B. Márquez, S.A. Brandán, Int. J. Quant. Chem. 114 (2014) 209–221.
[4] A.B. Raschi, E. Romano, M.V. Castillo, P. Leyton, C. Paipa, L.M. Maldonado, S.A. Brandán, Vib. Spectrosc. 70 (2014) 100–109.
[5] K.-J. Lee, K. Dabrowski, M.M. Sandoval, J.S. Mark, Aquaculture 244 (2005) 293–301.
[6] M. Sandoval, N.N. Okuhama, F.M. Angeles, V.V. Melchor, L.A. Condezo, J. Lao, M.J.S. Miller, Food Chem. 79 (2002) 207–213.
[7] K. Valentova, D. Buckiova, V. Kren, J. Peknicova, J. Ulrichova, V. Simanek, Cell Biol. Toxicol. 22 (2) (2006) 91–99.
[8] Y. Zhang, L. Yu, M. Ao, W. Jin, J. Ethnopharmacol. 105 (1–2) (2006) 274–279.
[9] Y. Wang, Y. Wang, B. McNeil, L.M. Harvey, Food Res. Int. 40 (7) (2007) 783–792.
[10] A.F.G. Cicero, E. B., R. Arletti, J. Ethnopharmacol. 75 (2001) 225–229.
[11] B.L. Zheng, K.H., C.H. Kim, L. Rogers, Y. Shao, Z.Y. Huang, Y. Lu, S.J. Yan, L.C. Qien, Q.Y. Zheng, Urology 55 (4) (2000) 598–602.
[12] G.F. Gonzales, A.C., K. Vega, A. Chung, A. Villena, C. Góñez, J. Endocrinol. 176 (2003) 163–168.
[13] A.J. Jin, H. Kohn, C. Béguin, S.V. Andurkar, J.P. Stables, D.F. Weaver, Can. J. Chem. 83 (1) (2005) 37–45.
[14] W.H. Prichard, Detection and Determination of Acid Derivatives, in: S. Patai (Ed.), Acid Derivatives, 1, John Wiley & Sons, Ltd, Chichester, UK, 1979.
[15] I. Muhammad, J. Z., D.C. Dunbar, I.A. Khan, Phytochem. 59 (2002) 105–110.
[16] I. Dini, G.C. T., A. Dini, Biochem. Syst. Ecol. 2002 (2002) 1087–1090.
[17] M.R. Tellez, I.A.K. Mozaina Kobaisy, K.K. Schrader, F.E. Dayan, W. Osbrink, Phytochemistry 61 (2002) 149–155.
[18] S. Piacente, V.C., A. Plaza, A. Zampelli, C. Pizza, J. Agri. Food Chem. 50 (2002) 5621–5625.
[19] B. Cui, B.L.Z., K. He, Q.Y. Zheng, J. Nat. Prod. 66 (2003) 1101–1103.
[20] J. Zhao, I.M.,D.C. Dunbar, J. Mustafa, I.A. Khan, J. Agric. Food Chem. 53 (3) (2005) 690–693.
[21] F.E. Chain, A. Grau, J.C. Martins, C.A.N. Catalán, Phytochem. Lett. 8 (2014) 145–148.
[22] S. Dapprich, I. Komáromi, K.S. Byun, K. Morokuma, M.J. Frisch, J. Mol. Struct. (Theochem) 462 (1999) 1–21.
[23] A.D. Becke, J. Chem. Phys. 98 (1993) 5648–5652.
[24] C. Lee, W. Yang, R.G. Parr, Phys. Rev. B37 (1988) 785–789.

[25] A.E. Reed, L.A. Curtis, F. Weinhold, Chem. Rev. 88 (6) (1988) 899–926.
[26] E.D. Glendening, J.K. Badenhoop, A.D. Reed, J.E. Carpenter, F. Weinhold, NBO 3.1, Theoretical Chemistry Institute, University of Wisconsin, Madison, WI, 1996.
[27] R.F.W. Bader, Atoms in Molecules. A Quantum Theory,, Oxford University Press, Oxford, 1990, ISBN 0198558651.
[28] F. Biegler-Köning, J. Schönbohm, D.J. Bayles, Comput. Chem. 22 (2001) 545–559.
[29] R.G. Parr, R.G. Pearson, J. Am. Chem. Soc. 105 (1983) 7512–7516.
[30] a) G. Rauhut, P. Pulay, J. Phys. Chem. 99 (1995) 3093–3099;
b) G. Rauhut, P. Pulay, J. Phys. Chem. 99 (1995) 14572.
[31] T. Sundius, Vib. Spectrosc.. 29, 89–95.
[32] A.B. Nielsen, A.J. Holder, Gauss view 5.0, User's Reference, GAUSSIAN Inc., Pittsburgh, PA, 2008.
[33] M.J. Frisch, G. W. Trucks, H.B. Schlegel, G.E. Scuseria, M.A. Robb, J.R. Cheeseman, G. Scalmani, V. Barone, B. Mennucci, G.A. Petersson, H. Nakatsuji, M. Caricato, X. Li, H.P. Hratchian, A.F. Izmaylov, J. Bloino, G. Zheng, J.L. Sonnenberg, M. Hada, M. Ehara, K. Toyota, R. Fukuda, J. Hasegawa, M. Ishida, T. Nakajima, Y. Honda, O. Kitao, H. Nakai, T. Vreven, J.A. Montgomery, Jr., J.E. Peralta, F. Ogliaro, M. Bearpark, J.J. Heyd, E. Brothers, K. N. Kudin, V.N. Staroverov, R. Kobayashi, J. Normand, K. Raghavachari, A. Rendell, J.C. Burant, S.S. Iyengar, J. Tomasi, M. Cossi, N. Rega, J.M. Millam, M. Klene, J.E. Knox, J.B. Cross, V. Bakken, C. Adamo, J. Jaramillo, R. Gomperts, R.E. Stratmann, O. Yazyev, A.J. Austin, R. Cammi, C. Pomelli, J.W. Ochterski, R.L. Martin, K. Morokuma, V.G. Zakrzewski, G.A. Voth, P. Salvador, J.J. Dannenberg, S. Dapprich, A.D. Daniels, O. Farkas, J.B. Foresman, J.V. Ortiz, J. Cioslowski, and D.J. Fox, Gaussian, Inc., Wallingford CT, 2009.
[34] R. Ditchfield, Mol. Phys. 8 (1974) 397–409.
[35] Ming-Shi Wang, Lib Hai-Yan, Wu Wei-Na, Acta Cryst. E67 (2011) o1558.
[36] W. Smiszek-Lindert, J. Kusz, Acta Cryst. E63 (2007) o3713.
[37] L. Tapia, J. Torres, L. Mendoza, A. Urzúa, J. Ferreira, M. Pavani, M. Wilkens, Planta Med. 70 (11) (2004) 1058–1063.
[38] K.V. Sashidhara, J.N. Rosaiah, A. Kumar, H.K. Bid, R. Konwar, N. Chattopadhyay, Phytother. Res. 21 (11) (2007) 1105–1108.
[39] A. Urzúa, M.C. Rezende, C. Mascayano, L. Vásquez, Molecules 13 (2008) 882–891.
[40] E. Lizarraga, E. Romano, A.B. Raschi, P. Leyton, C. Paipa, S.A. Brandán, J. Mol. Struct. 1048 (2013) 331–338.
[41] F. Chain, E. Romano, P. Leyton, C. Paipa, C.A.N. Catalán, M.A. Fortuna, S.A. Brandán, J. Mol. Struct. 1065–1066 (2014) 160–169.
[42] B.H. Besler, K.M. Merz Jr., P.A. Kollman, J. Comp. Chem. 11 (1990) 431–439.
[43] Y. Wang, W.-N. Wu, R.-Q. Zhao, A.-Y. Zhang, B.-F. Qin, Acta Cryst. E66 (2010) m292.
[44] J.-L. Bredas, Mater. Horiz. 1 (2014) 17–19.
[45] NIST Chemistry WebBook (http//webbook.nist.gov/chemistry).
[46] P.G. Cataldo, M.V. Castillo, S.A. Brandán, J. Phys. Chem. Biophys. 4 (1) (2014) 4–9.
[47] P. Leyton, C. Paipa, A. Berrios, A. Zárate, S. Fuentes, M.V. Castillo, S.A. Brandán, J. Mol. Struct. 1031 (2013) 110–118.
[48] T.J. Bruno, P.D.N. Svoronos, CRC Handbook of Basic Tables for Chemical Analysis, second ed., CRC Press, Taylor & Francis Group, Boca Raton, 2011.
[49] R.A. Friedel, M. Orchin, Ultraviolet Spectra of Aromatic Compounds, Wiley & Sons, New York and London, 1951.